INTERNATIONAL JOURNAL OF
Minerals, Metallurgy and Materials

Volume 31, Number 2, February 2024
Page 231

Invited Review https://doi.org/10.1007/s12613-023-2761-z

Recent progress on Sn_3O_4 nanomaterials for photocatalytic applications

Xin Yu[1),✉], *Congcong Li*[2)], *Jian Zhang*[3)], *Lili Zhao*[1)], *Jinbo Pang*[1)], *and Longhua Ding*[1),✉]

1) Institute for Advanced Interdisciplinary Research (iAIR), School of Chemistry and Chemical Engineering, University of Jinan, Jinan 250022, China
2) School of Sino-German Engineering, Shanghai Technical Institute of Electronics and Information, Shanghai 201411, China
3) Division of Systems and Synthetic Biology, Department of Life Sciences, Chalmers University of Technology, 412 96 Göteborg, Sweden

(Received: 23 May 2023; revised: 21 July 2023; accepted: 10 October 2023)

Abstract: Tin(IV) oxide (Sn_3O_4) is layered tin and exhibits mixed valence states. It has emerged as a highly promising visible-light photocatalyst, attracting considerable attention. This comprehensive review is aimed at providing a detailed overview of the latest advancements in research, applications, advantages, and challenges associated with Sn_3O_4 photocatalytic nanomaterials. The fundamental concepts and principles of Sn_3O_4 are introduced. Sn_3O_4 possesses a unique crystal structure and optoelectronic properties that allow it to absorb visible light efficiently and generate photoexcited charge carriers that drive photocatalytic reactions. Subsequently, strategies for the control and improved performance of Sn_3O_4 photocatalytic nanomaterials are discussed. Morphology control, ion doping, and heterostructure construction are widely employed in the optimization of the photocatalytic performance of Sn_3O_4 materials. The effective implementation of these strategies improves the photocatalytic activity and stability of Sn_3O_4 nanomaterials. Furthermore, the review explores the diverse applications of Sn_3O_4 photocatalytic nanomaterials in various fields, such as photocatalytic degradation, photocatalytic hydrogen production, photocatalytic reduction of carbon dioxide, solar cells, photocatalytic sterilization, and optoelectronic sensors. The discussion focuses on the potential of Sn_3O_4-based nanomaterials in these applications, highlighting their unique attributes and functionalities. Finally, the review provides an outlook on the future development directions in the field and offers guidance for the exploration and development of novel and efficient Sn_3O_4-based nanomaterials. Through the identification of emerging research areas and potential avenues for improvement, this review aims to stimulate further advancements in Sn_3O_4-based photocatalysis and facilitate the translation of this promising technology into practical applications.

Keywords: photocatalysis; Sn_3O_4 nanomaterials; building heterostructures; antibacterial therapy; water splitting

1. Introduction

Scientific research focuses on solar energy due to environmental and energy challenges. Photocatalysis is pivotal in the conversion of solar light energy to chemical energy, making it an important research field. Compared with traditional semiconductor photocatalysts such as metal oxide [1], metal-organic frameworks (MOFs) [2–3], and covalent organic frameworks (COFs) [4], tin oxides have been extensively investigated due to their abundant availability, nontoxic nature, and remarkable optical and electrical properties [5–7]. The stable stannic oxide (SnO_2) and the metastable SnO [8] are the most common tin oxide compounds encountered in nature. SnO_2 is an n-type wide-bandgap semiconductor with rutile and cassiterite structures [9]. SnO is a p-type semiconductor with a bandgap ranging from 2.5 to 3.4 eV and naturally exists in three crystallographic forms, including α-SnO with a cubic crystal structure, β-SnO with a tetragonal crystal structure, and γ-SnO. Over the past decades, SnO_2 and SnO have been extensively applied in areas such as lithium-ion batteries, solar cells, gas sensors, and photocatalysis, owing to their exceptional electrical and optical properties [10–11].

Certain nonstoichiometric tin oxides, including Sn_2O_3, Sn_3O_4, and Sn_5O_6, present unique physicochemical properties, such as magnetism and electrochemical performance [12]. Generally, tin oxides display diverse oxidation states derived from Sn, notably Sn^{2+} and Sn^{4+}. SnO_2 has been intensively studied due to its low resistance, high optical transparency, multivalence surfaces, and conductivity variations induced by adsorbates. These features have paved the way for the wide application of SnO_2 in transparent conductors, oxide catalysis, and solid-state gas sensors [13]. Moreover, the relatively deep valence band (VB) position of SnO_2 has resulted in its exploration as a photocatalyst for organic compounds such as methylene blue (MB) [14]. SnO is used as a reducing agent in cranberry glass production, and it is used as anode and coating materials in rechargeable lithium-ion batteries (LIBs) [15]. The p-type conductivity exhibited by SnO is a rare characteristic among metal oxide materials [16].

The mixed valence tin oxide, Sn_3O_4, has attracted considerable interest in the fields of photocatalysis, electrocatalysis, and photoelectrocatalysis [17–18]. The coexistence of Sn^{2+} and Sn^{4+} narrows its bandgap, imparting a yellowish hue to the material and enabling it to absorb visible light [19–20].

✉ Corresponding authors: Xin Yu E-mail: ifc_yux@ujn.edu.cn; Longhua Ding E-mail: bio_dinglh@ujn.edu.cn

Springer

Tanabe *et al.* [21] extensively investigated single-phase Sn_3O_4 synthesized via hydrothermal methods, focusing on its application as a photocatalyst for water splitting and CO_2 reduction. The various types of the tin oxide family feature distinct physical and chemical properties, which render them scientifically intriguing and suitable for a wide range of technological applications [22]. However, the chemical composition of tin oxides extends beyond the two initially described compounds. Besides Sn_3O_4, other forms of Sn_xO_y ($0.5 < x/y < 1$), such as Sn_2O_3, Sn_4O_5, and Sn_5O_6, have been proposed, but their structures and stability remain debatable [23–24]. Consequently, computational studies have been conducted to predict the structure and property of these tin oxides, and the related calculations have been validated.

This review article presents the latest overview of recent advancements in the field of Sn_3O_4 photocatalytic nanomaterials. The article first introduces the crystal structure and property of Sn_3O_4, providing a solid foundation for the comprehension of its photocatalytic behavior. Subsequently, the comprehensive summary of various approaches for the enhancement of the photocatalytic activity of Sn_3O_4 are focused such as morphology control, ion doping, and heterostructure construction. Moreover, the diverse applications of Sn_3O_4 photocatalytic materials are discussed, with a focus on areas such as photocatalytic degradation, photocatalytic hydrogen production, carbon dioxide reduction, antibacterial treatment, and optoelectronic sensing. A thorough discussion centers on the potential of Sn_3O_4-based nanomaterials in these applications, highlighting their unique properties and capabilities. Lastly, the article presents the future development directions in the field, offering valuable insights and guidance for the exploration and advancement of novel and highly efficient Sn_3O_4-based nanomaterials. Key areas of focus and potential research directions are also outlined to stimulate further progress and innovations in the field of Sn_3O_4 photocatalysis.

2. Structure and characteristics of Sn_3O_4

Sn_3O_4 is a thermodynamically stable intermediate compound within the Sn–O phase diagram, and it exists in two distinct phases, the stable α phase and the unstable β phase (Fig. 1(a)) [23]. Sn_3O_4 has a crystal structure of layered arrangement, with alternating stacked layers of symmetric SnO_6 octahedra and distorted SnO-like units at the interfaces between layers. According to theoretical calculations, the coexistence of Sn^{2+} and Sn^{4+} in Sn_3O_4 leads to an optimal band structure for photocatalytic hydrogen evolution, which is characterized by a bandgap that aligns correspondingly with the energy of visible-light photons.

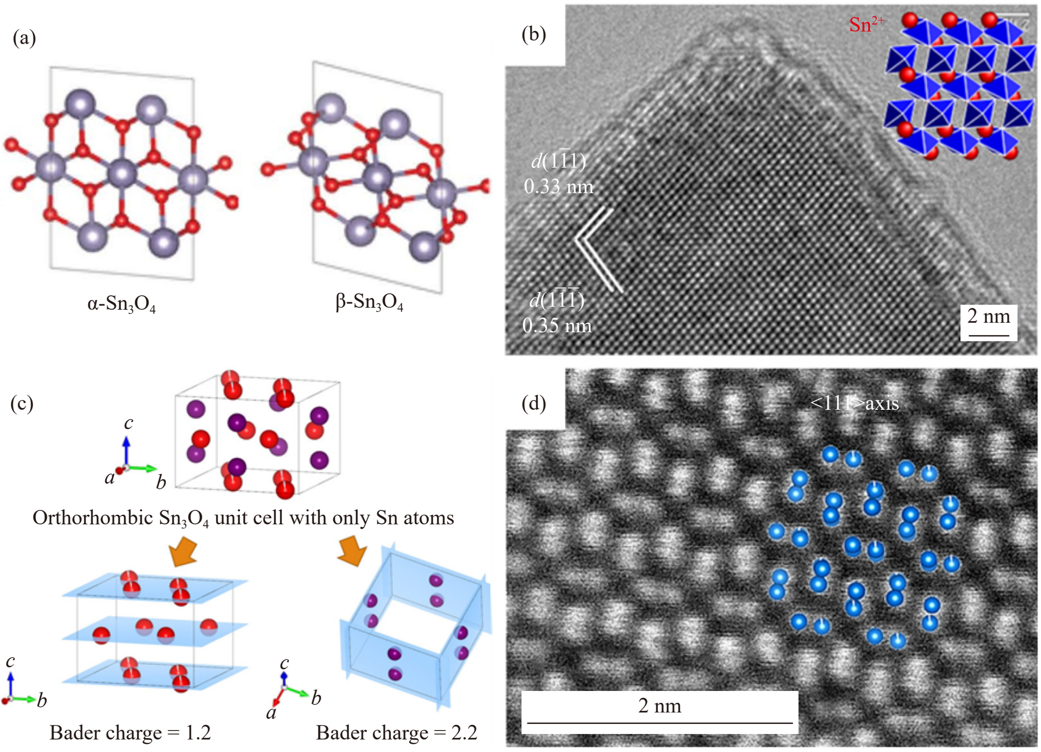

Fig. 1. (a) Crystal structure of α-Sn_3O_4 and β-Sn_3O_4. J.J. Wang, N. Umezawa, and H. Hosono, *Adv. Energy Mater.*, 6, 1501190 (2016) [23]. Copyright Wiley-VCH Verlag GmbH & Co. KGaA. Reproduced with permission; (b) high-resolution transmission electron microscopy (HRTEM) image of Sn_3O_4. Reprinted with permission from M. Manikandan, T. Tanabe, P. Li, *et al.*, *ACS Appl. Mater. Interfaces*, 6, 3790 [24]. Copyright 2014 American Chemical Society; (c) schematic of Bader charge analysis (blue planes added for better visualization): unit cell of orthorhombic Sn_3O_4 with tin atoms only, tin atoms with a Bader charge around 1.2 (red) at the 4g and 4h Wyckoff positions and 2.2 (purple) at the 4f Wyckoff positions; (d) high-angle annular dark-field scanning transmission electron microscopy (HAADF-STEM) image of orthorhombic Sn_3O_4. Y.S. Liu, A. Yamaguchi, Y. Yang, *et al.*, *Angew. Chem. Int. Ed.*, 62, e202300640 (2023) [25]. Copyright Wiley-VCH Verlag GmbH & Co. KGaA. Reproduced with permission.

Manikandan *et al.* [24] fabricated nanoscale structures comprising Sn_3O_4 nanosheets (Fig. 1(b)). In conjunction with Pt as a cocatalyst, the Sn_3O_4 material displayed a notable catalytic performance in the visible-light-driven decomposition of water within aqueous solutions. To optimize the synthesis of monoclinic phase Sn_3O_4, Liu *et al.* [25] systematically investigated various parameters, including heating time, pH, solution composition, and washing methods. Furthermore, the synthesis was controlled with precision through the modulation of the filling level of the precursor solution and tailoring of the gas composition within the hydrothermal reactor. Their study successfully unveiled a novel phase of Sn_3O_4 possessing a structure similar to the orthorhombic $SnPb_2O_4$ (Fig. 1(c)–(d)). Notably, a narrower bandgap was observed in the orthorhombic Sn_3O_4 polymorph compared with the conventional monoclinic Sn_3O_4 phase, which implies the enhanced absorption and utilization of visible light in photocatalytic devices.

3. Synthesis of Sn_3O_4

The synthesis strategies for Sn_3O_4 can be broadly classified into two main categories. Solid-phase methods encompass annealing and carbothermal approaches, and liquid-phase methods include hydrothermal and solvothermal techniques [26–28]. Annealing is the earliest successfully applied method, and it entails heating of SnO to influence the transformation of unstable divalent tin to its tetravalent form, yielding a mixed-valence tin oxide. On the other hand, the carbothermal method employs carbon powder as a reducing agent to reduce SnO_2 at elevated temperature, which leads to the formation of Sn_3O_4. Meanwhile, solid-phase approaches are used to synthesize Sn_3O_4 with diverse morphologies, and they often necessitate stringent and time-consuming experimental conditions, resulting in suboptimal sample purity. Conversely, liquid-phase methods, such as hydrothermal or solvothermal routes, offer a comparatively simple, safe, and controllable means of fabricating Sn_3O_4 nanomaterials [29–30]. For these methods, at specific temperature and pressure conditions, a precursor reactant undergoes a reaction within a reaction vessel lined with polytetrafluoroethylene in a sealed system with either water or organic solvent as the solution. allowing for the precise control of nucleation and growth processes for the production of Sn_3O_4 nanomaterials with diverse morphologies. The synthesized products exhibit excellent crystallinity, a relatively uniform grain distribution, and notable advantages, including the absence of agglomeration and the elimination of the need for calcination.

4. Strategies for improving photocatalytic performance

4.1. Mechanisms of photocatalytic enhancement

Semiconductor photocatalysis relies on the principles of solid-state band structures [31–32]. Sn_3O_4 is an exemplary n-type semiconductor with a band structure comprising an unoccupied high-energy conduction band (CB), a filled VB with electrons, and a bandgap separating the two [33]. Sn_3O_4 is an indirect bandgap semiconductor, which means that the excitation of electrons from the VB to the CB occurs when the energy of incident light matches or surpasses the bandgap energy of Sn_3O_4. This process initiates the generation of highly active electron–hole pairs within the VB. However, the photogenerated electrons and holes are susceptible to recombination, dissipating stored light energy as heat in the absence of suitable electron or hole capture agents or driving forces. The appropriate acceptors or defects present on the catalyst's surface can suppress the recombination of photogenerated charge carriers, which facilitates their efficient separation and transfer to distinct sites on the surface. Photogenerated holes possess outstanding oxidation capabilities, whereas electrons are known for their strong reduction capacities. Consequently, photogenerated holes can oxidize water on the surface of Sn_3O_4, forming hydroxyl radicals ($\cdot OH$). Meanwhile, electrons engage in reactions involving the dissolved oxygen adsorbed on the surface, yielding superoxide radicals ($\cdot O_2^-$). These active species exhibit potent oxidation capabilities, which enable the complete mineralization of various organic pollutants into uncontaminated water and carbon dioxide [34]. In addition, highly active photogenerated electrons and holes can interact with water and liberating hydrogen and oxygen [35].

4.2. Strategies for photocatalytic enhancement

Certain challenges have been associated with single-phase Sn_3O_4 photocatalytic materials: (1) Conventional synthesis methods typically yield single-phase Sn_3O_4 materials, leading to elevated recombination rates of photogenerated charge carriers that detrimentally affect the photocatalytic performance. (2) Solar energy utilization remains suboptimal. Visible light energy constitutes approximately 44% of the solar spectrum, with near-infrared light accounting for roughly 50% [36]. Sn_3O_4 can only absorb a small portion of visible light (<500 nm) [30]. Consequently, recent extensive research has concentrated on the expansion of the light absorption range of photocatalytic materials, which facilitated the efficient separation of photogenerated charge carriers and further enhanced their photocatalytic capabilities. These research endeavors primarily involved morphology control, ion doping, and the construction of heterostructures using Sn_3O_4 materials.

4.2.1. Morphological control

Semiconductor materials with different morphologies and particle sizes exhibit distinct physicochemical properties, which often influence their photocatalytic performance through variations in the specific surface area and crystal facet exposure [11,37]. In general, small particles possess large specific surface areas and follow short migration paths for photoinduced charges, thereby favoring improved photocatalytic activity. Furthermore, when the particle size approaches the radius of the first exciton (i.e., 1–10 nm), quantum size effects can be observed. These effects result in a widened bandgap and enhance the catalytic capability of photoinduced electrons and holes and photocatalytic performance. Similar trends have been observed in Sn_3O_4 photocatalytic materials. Stable structures of Sn_3O_4 nanostructures, such as nanobelts [38], nanowires (NWs) [39], nanoflowers [40], and microball [41], have been prepared successfully through the selection of appropriate precursors and precise control of reaction conditions (Fig. 2).

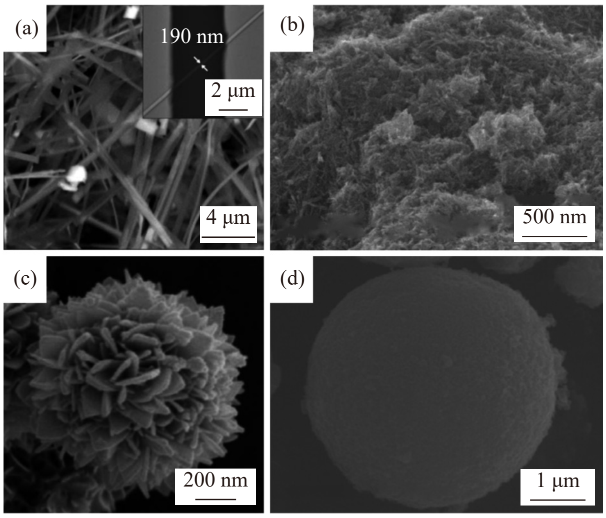

Fig. 2. Scanning electron microscopy (SEM) images of Sn_3O_4 with different morphologies: (a) nanobelts. Reprinted with permission from O.M. Berengue, R.A. Simon, A.J. Chiquito, *et al.*, *J. Appl. Phys.*, 107, 033717 (2010) [38]. Copyright 2010 AIP Publishing LLC; (b) NWs. Reprinted from *Nano Struct. Nano Objects*, 24, P. Mone, S. Mardikar, and S. Balgude, Morphology-controlled synthesis of Sn_3O_4 nanowires for enhanced solar-light driven photocatalytic H_2 production, 100615, Copyright 2020, with permission from Elsevier; (c) nanoflower. Republished with permission of Royal Society of Chemistry, from Sn_3O_4: A novel heterovalent-tin photocatalyst with hierarchical 3D nanostructures under visible light, Y.H. He, D.Z. Li, J. Chen, *et al.*, 4, 2013; permission conveyed through Copyright Clearance Center, Inc; (d) microball. Reprinted from *Mater. Chem. Phys.*, 221, S. Balgude, Y. Sethi, B. Kale, D. Amalnerkar, and P. Adhyapak, Sn_3O_4 microballs as highly efficient photocatalyst for hydrogen generation and degradation of phenol under solar light irradiation, 493, Copyright 2019, with permission from Elsevier.

He *et al.* [40] synthesized a three-dimensional (3D) hierarchical nanostructured Sn_3O_4 photocatalyst using a template-free solvothermal method. SnO_2, Sn_3O_4, and SnO were obtained by adjusting the pH of the suspension. Specifically, white SnO_2 nanoparticles were prepared at pH = 1, pure Sn_3O_4 with a yellow color formed at pH = 3, and black SnO was synthesized under alkaline conditions with a pH of 13. Damaschio *et al.* [26] synthesized single-crystalline Sn_3O_4 nanobelts, which grew via a gas–solid mechanism through a carbon thermal reduction process. Electrical measurements of individual Sn_3O_4 nanobelts at different temperatures revealed the characteristics of undoped semiconductors. Balgude *et al.* [41] used an amber salt-driven hydrothermal method to synthesize Sn_3O_4 microspheres. These microspheres displayed an irregular contour nanostructure with thicknesses ranging from approximately 40 to 80 nm and excellent photocatalytic hydrogen production and phenol degradation activity under solar light irradiation. Mone *et al.* [39] applied a simple apple acid-induced hydrothermal process to synthesize Sn_3O_4 NWs with an exceptional hydrogen evolution activity using tin oxalate as the starting material. The NWs exhibited a higher photocatalytic activity than their nanosheets counterparts, which could be attributed to the layered morphology and high crystallinity of Sn_3O_4 NWs. Through precise control of the morphology, Sn_3O_4 nanostructures with large specific surface areas were prepared, along with the exposure of more active sites and promoted photocatalytic activity.

4.2.2. Ion doping

Ionic doping is an early proposed strategy for catalyst modification. In this method, metallic or nonmetallic ions are introduced into the lattice structure of the catalyst [42–46]. This doping approach broadens a material's absorption spectrum and creates charge separation centers that suppress the recombination of photogenerated charge carriers. Metallic ion doping introduces new charges, induces defects, alters lattice type, affects the movement and distribution of photogenerated electrons and holes, and modifies the band structure of Sn_3O_4, ultimately leading to changes in photocatalytic activity. Yang *et al.* [47] synthesized nickel-doped Sn_3O_4 (Ni-Sn_3O_4) using a one-pot synthesis method, which enabled the successful incorporation of metallic Ni into the lattice of Sn_3O_4. The doped Ni acted as a crystallinity inducer and enhanced the crystal quality of Sn_3O_4. Remarkably, under visible-light illumination, Ni-Sn_3O_4 exhibited considerably improved photocatalytic hydrogen evolution performance, which is approximately 3.4 times higher than that of pure-phase Sn_3O_4. This enhanced activity was primarily attributed to the improved crystallinity of Ni-Sn_3O_4. Ni doping effectively reduced the bandgap width, enhancing light absorption, and increasing the susceptibility of the material to visible-light excitation (Fig. 3(a)).

Nonmetal ion doping effectively extends the light absorption range of Sn_3O_4 materials and enables the direct utilization of a substantial portion of solar energy, including visible and near-infrared light. The nonmetal elements nitrogen (N), sulfur, carbon, and halogens are commonly used in doping. Balgude *et al.* [43] synthesized N-doped Sn_3O_4 (N-Sn_3O_4) using urea as the N precursor. The introduction of N led to the formation of new N 2p band on the O 2p VB, resulting in bandgap narrowing and the expansion of the light absorption edge to a wider range in the visible-light region (Fig. 3(b)). Furthermore, Zeng *et al.* [44] reported the effect of novel fluorine-doped Sn_3O_4 (F-Sn_3O_4) on the removal of pollutants in water, particularly the reduction of Cr(VI) and the degradation of organic pollutants. They demonstrated that F doping in Sn_3O_4 enhanced the redox potential, which led to the generation of more electron–hole pairs and facilitated the separation of photoinduced electron–hole pairs. As a result, more reactive oxygen species (ROS) were produced.

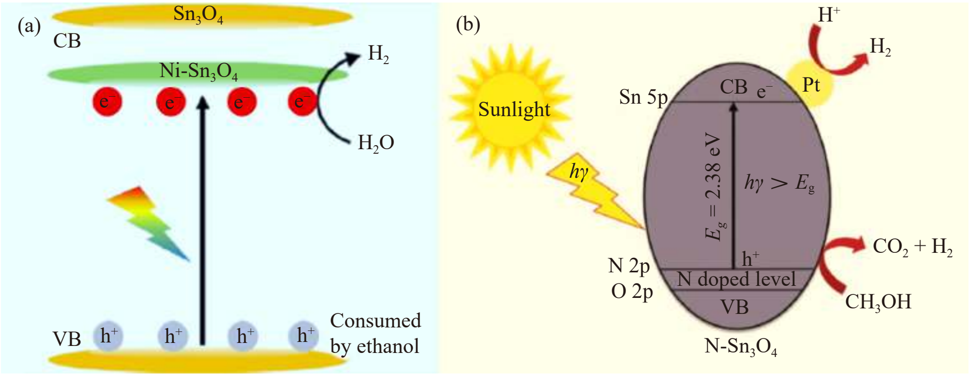

Fig. 3. (a) Band alignment of Sn_3O_4 and Ni-Sn_3O_4. Reprinted with permission from R.Q. Yang, Y.C. Ji, L.W. Wang, *et al.*, *ACS Appl. Nano Mater.*, 3, 9268 [47]. Copyright 2020 American Chemical Society; (b) possible mechanism for photocatalytic hydrogen production by N-Sn_3O_4 under sunlight irradiation. Republished with permission of Royal Society of Chemistry, from Unique N doped Sn_3O_4 nanosheets as an efficient and stable photocatalyst for hydrogen generation under sunlight, S. Balgude, Y. Sethi, A. Gaikwad, B. Kale, D. Amalnerkar, and P. Adhyapak, 12, 2020; permission conveyed through Copyright Clearance Center.

4.2.3. Heterostructures

The construction of heterostructures expands light absorption properties and enhances the charge carrier separation capabilities of materials [35–36,48–50]. Interface band engineering enables the formation of heterostructures between Sn_3O_4 and various components, such as metal particles, inorganic semiconductors, organic semiconductors, carbon materials, and others [51–52]. Yang *et al.* [53] achieved an *in-situ* reduction of Sn_3O_4 under a H_2 atmosphere and precisely controlled the reduction temperature and duration to create oxygen vacancies in Sn_3O_{4-x}. In addition, a portion of Sn_3O_4 was reduced to Sn nanoparticles, which led to the formation of semiconductor–metal contact in the Sn_3O_{4-x}/Sn Schottky junction. The Schottky junction was also established between Sn_3O_{4-x} and Sn, and it effectively enhanced the separation of photogenerated charge carriers. Meanwhile, the Schottky junction at the interface reduced the recombination of photogenerated charge carriers, and the excellent conductivity of Sn metal facilitated electron transfer. This synergistic effect considerably improved the utilization of light energy, resulting in the outstanding photocatalytic performance of the Sn_3O_{4-x}/Sn composite photocatalytic material (Fig. 4(a)).

Furthermore, Yu *et al.* [33] successfully fabricated a 3D semiconductor–semiconductor Janus-type heterostructure

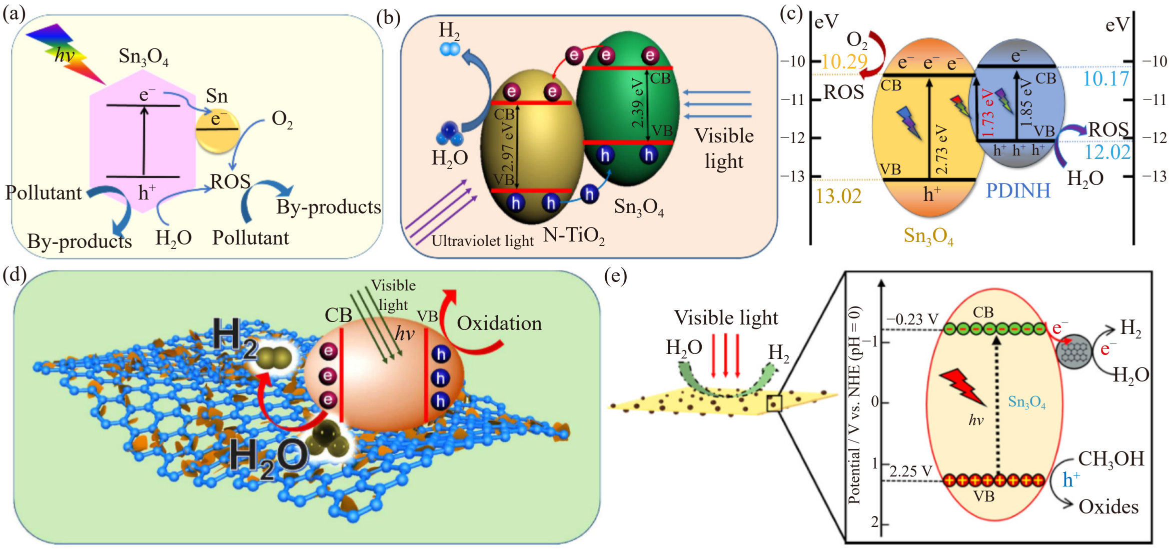

Fig. 4. Schematic of the band structure and photoinduced charge transfer and separation at the interface: (a) Sn_3O_4/Sn. Reprinted by permission from Springer Nature: *Int. J. Miner. Metall. Mater.*, Sn/Sn_3O_{4-x} heterostructure rich in oxygen vacancies with enhanced visible light photocatalytic oxidation performance, R.Q. Yang, N. Liang, X.Y. Chen, *et al.*, Copyright 2021; (b) Sn_3O_4/TiO_2. Republished with permission of Royal Society of Chemistry, from Hierarchical hybrid nanostructures of Sn_3O_4 on N doped TiO_2 nanotubes with enhanced photocatalytic performance, X. Yu, L.F. Wang, J. Zhang, *et al.*, 3, 2015; permission conveyed through Copyright Clearance Center; (c) Sn_3O_4/PDINH. R.Q. Yang, G.X. Song, L.W. Wang, *Small*, 17, e2102744 (2021) [29]. Copyright Wiley-VCH Verlag GmbH & Co. KGaA. Reproduced with permission; (d) Sn_3O_4/rGO. Reprinted from *Appl. Catal. B Environ.*, 227, X. Yu, Z.H. Zhao, D.H. Sun, *et al.*, Microwave-assisted hydrothermal synthesis of Sn_3O_4 nanosheet/rGO planar heterostructure for efficient photocatalytic hydrogen generation, 470, Copyright 2018, with permission from Elsevier; (e) Sn_3O_4/GQDs heterostructure. Reprinted with permission from X. Yu, Z.H. Zhao, N. Ren, *et al.*, *ACS Sustainable Chem. Eng.*, 6, 11775 [56]. Copyright 2018 American Chemical Society.

photocatalyst of Sn_3O_4/N-TiO_2 by electrospinning and hydrothermal methods . The contact made by Sn_3O_4 with the outer shell of N-TiO_2 nanotubes led to the formation of a heterostructure. Photogenerated holes and electrons emerged in the VB and CB of N-TiO_2 and Sn_3O_4, respectively. Given the distinct band positions of N-TiO_2 and Sn_3O_4, photogenerated electrons in the CB of Sn_3O_4 were readily injected into the CB of TiO_2, and the holes in the VB of TiO_2 were injected into the VB of Sn_3O_4. In addition, the unique Janus morphology of Sn_3O_4/N-TiO_2 contributed to the synergistic effect between the band structure and morphology, facilitating the effective separation of photogenerated electron–hole pairs (Fig. 4(b)).

Organic semiconductors refer to a class of organic materials possessing semiconductor properties and exhibiting favorable characteristics, such as good conductivity, nontoxicity, ease of fabrication, high stability, and unique electrochemical and physical properties. Polyaniline (PANI) and perylene diimide (PDI) are commonly used organic semiconductors. Yang *et al.* [29] successfully prepared a Sn_3O_4/pyromellitic diimide (PDINH) heterostructure by depositing a 5 nm-thick PDINH layer onto the surface of Sn_3O_4 through recrystallization (Fig. 4(c)). Under illumination, three key processes occurred: (I) Sn_3O_4 absorbed light below 450 nm, generating electron–hole pairs; (II) PDINH absorbed light below 670 nm, which also generated electron–hole pairs; (III) Sn_3O_4 and PDINH formed a heterostructure via interfacial interaction, and given their favorable band alignment, electrons transitioned from the VB of PDINH to the CB of Sn_3O_4. This heterostructure exhibited a bandgap of 1.73 eV, extending the light absorption range to approximately 720 nm and notably enhancing the utilization of solar energy.

Moreover, Sn_3O_4 can form heterostructures with carbon materials such as reduced graphene oxide (rGO). rGO, known for its high surface area and excellent conductivity, is widely used in combination with various semiconductor photocatalysts [54–55]. A microwave-assisted hydrothermal method enables the synthesis of a planar heterostructure consisting of Sn_3O_4 nanosheets and rGO [30]. The adoption of the microwave-assisted hydrothermal method considerably reduces the reaction time, allowing the uniform growth of Sn_3O_4 nanosheets on rGO. Under visible-light illumination, photogenerated holes and electrons appeared in the VB and CB of Sn_3O_4, respectively. Typically, these charge carriers recombined rapidly, leading to a low photocatalytic hydrogen evolution rate of Sn_3O_4 alone. However, when Sn_3O_4 nanoparticles were anchored onto the surface of rGO, the photogenerated electrons in the CB of Sn_3O_4 transferred to rGO, facilitating hole-electron separation. rGO acted as an electron collector and transporter, effectively prolonging the lifetime of charge carriers and thereby enhancing charge separation and photocatalytic activity (Fig. 4(d)).

Furthermore, graphene can be reduced in size to form graphene quantum dots (GQDs), which exhibit unique capabilities, such as photoinduced electron transfer, photoluminescence, and electron storage, while maintaining a 2D structure. Under visible-light irradiation, electrons in the Sn_3O_4/GQD heterostructure can be excited from the VB to the CB of Sn_3O_4 [56]. Subsequently, these electrons can transfer to GQDs, facilitating the effective separation of electron–hole pairs and enhancing photocatalytic activity. In addition, the π-conjugated GQDs function as sensitizers akin to organic dyes, sensitizing Sn_3O_4 to a broader range of visible-light absorption and providing electrons to the CB of Sn_3O_4, which leads to a more efficient visible-light-driven photocatalytic hydrogen production (Fig. 4(e)). Overall, these findings highlight the potential of Sn_3O_4-based heterostructures for the enhancement of photocatalytic activity and expansion of visible-light absorption range, paving the way for advanced applications in solar energy conversion.

5. Application of Sn_3O_4-based materials

5.1. Degradation of pollutants

The rapid development of industries has resulted in the crucial problem of water pollution for humans [20,44,57–58]. Yang *et al.* [59] successfully prepared a novel full-spectrum photocatalyst, Sn_3O_4/Ni foam heterostructure, via the *in situ* growth of Sn_3O_4 nanosheets on the surface of Ni foam. The porous structure of the Ni foam and the heterostructure that formed between Ni and Sn_3O_4 considerably enhanced the light absorption capacity of the photocatalyst.

Han *et al.* [60] introduced AgCl@Ag quantum dots to 2D Sn_3O_4 nanosheets at the oil–water interface to create a unique 3D flower-like structure of Sn_3O_4/AgCl@Ag composite photocatalyst. The synergistic combination of Sn_3O_4 with AgCl@Ag quantum dots enhanced the utilization of solar energy, and the heterostructure facilitated efficient photoinduced charge carrier transfer through the reduction of the energy barrier. The light-harvesting capacity of the material was further enhanced through surface plasmon resonance of Ag nanoparticles. Under visible-light irradiation, the photocatalytic activity of the Sn_3O_4/AgCl@Ag composite photocatalyst for the degradation of tetracycline hydrochloride and MB were 9.6 and 7.88 times, respectively, compared with that of pure Sn_3O_4 nanosheets. These findings demonstrate the potential of Sn_3O_4/AgCl@Ag composite photocatalysts for the efficient degradation of organic pollutants under visible light, paving the way for advanced water treatment technologies.

5.2. H_2 generation

H_2, as a clean and renewable energy source, plays a vital role in addressing the problems of environmental pollution and energy scarcity. Photocatalytic water splitting for hydrogen production is a crucial pathway [61–62]. Zou *et al.* [63] developed a Sn_3O_4/PPy heterostructure photocatalyst by employing a two-step process, which involved chemical oxidative polymerization and hydrothermal treatment for the *in-situ* immobilization of porous Sn_3O_4 nanosheets onto the hollow nanorods of polypyrrole (PPy) (Fig. 5(a)). The conductive PPy polymer modification facilitated the transfer of photogenerated electrons from the CB of Sn_3O_4 to PPy for water reduction and hydrogen production, and the holes were consumed by a methanol sacrificial agent at the VB of Sn_3O_4. In this system, PPy acted as an electron acceptor, initiating light-induced electron migration and promoting the separation of photogenerated electrons and holes, which improved the hydrogen generation performance of the Sn_3O_4/PPy heterostructure (Fig. 5(b)). In addition, the 3D structure formed by the uniform dispersion of porous Sn_3O_4 nanosheets on hollow PPy nanorods contributed to the improved performance. A remarkable photocatalyst hydrogen production rate of 481.05 $\mu mol\cdot g^{-1}$ was obtained within 5 h, and such value was 7.52 times higher than that of pure Sn_3O_4 (Fig. 5(c)).

Yang *et al*. [64] synthesized ultrafine Si NW arrays and *in-situ* grew Sn_3O_4 nanosheets on their surfaces (Fig. 5(d)). Combined with the light confinement effect of Sn_3O_4 nanosheets, the ultrafine NWs structure enhanced spectrum absorption. The formed heterostructure facilitated the direct transport of charge carriers, and the *in-situ* growth of Sn_3O_4 reduced the interface resistance during the efficient charge carrier transfer (Fig. 5(e)). Photocatalytic water splitting experiments were conducted to evaluate H_2 production under illumination, and the results revealed a remarkable increase in the generation of H_2 gas bubbles (Fig. 5(f)). Notably, the Si NW/Sn_3O_4 photoanodes, owing to the formation of a 3D heterostructure, exhibited significantly improved H_2 generation capability compared with the Si NWs (Fig. 5(g)). These findings underscore the potential of Si NW/Sn_3O_4 heterostructures as candidate photoanodes for enhanced H_2 production via photocatalytic water splitting.

5.3. Reduction of CO_2

The conversion of CO_2 to fuel with the use of solar light presents a promising solution for simultaneously addressing global warming and energy supply challenges. Chen *et al.* [65] conducted density functional theory calculations and experimental investigations and revealed Sn_3O_4 as the most effective electrocatalyst among SnO_x materials for the reduction of carbon-containing products under CO_2. The distinctive electronic structure of Sn_3O_4 enables synergistic effects between Sn^{2+} and Sn^{4+}, optimizing the adsorption strength of intermediates (Fig. 6(a)). Moreover, the upshifted band structure of Sn_3O_4 provides moderate adsorption energies for H and HCOO intermediates, suppresses hydrogen evolution reaction, and enhances the intrinsic catalytic efficiency of CO_2 reduction (Fig. 6(b)). The synthesized Sn_3O_4 electrocatalyst displayed a partial current density of 16.6 $mA\cdot cm^{-2}$ at −0.9 V vs. RHE and carbon-based Faradaic efficiency of approximately 97.7%. Notably, the overpotential (190 mV) is lower than that of most reported SnO_x-based electrocatalysts.

According to Liu *et al*. [66], under visible-light irradiation ($\lambda > 430$ nm), the synthesized Sn_3O_4 can catalyze the reduction of CO_2 to CO in aqueous solutions (Fig. 6(c)). Two different bubbling conditions were compared, and the findings revealed an increased CO production when CO_2 was bubbled, resulting in the generation of 0.16 μmol CO within 24 h (Fig. 6(d)). Furthermore, the rate of CO generation remained stable for 72 h (Fig. 6(e)). CO_2 reduction was environmentally friendly and stable due to the visible-light activity of Sn_3O_4, positioning it as a promising photocatalyst that

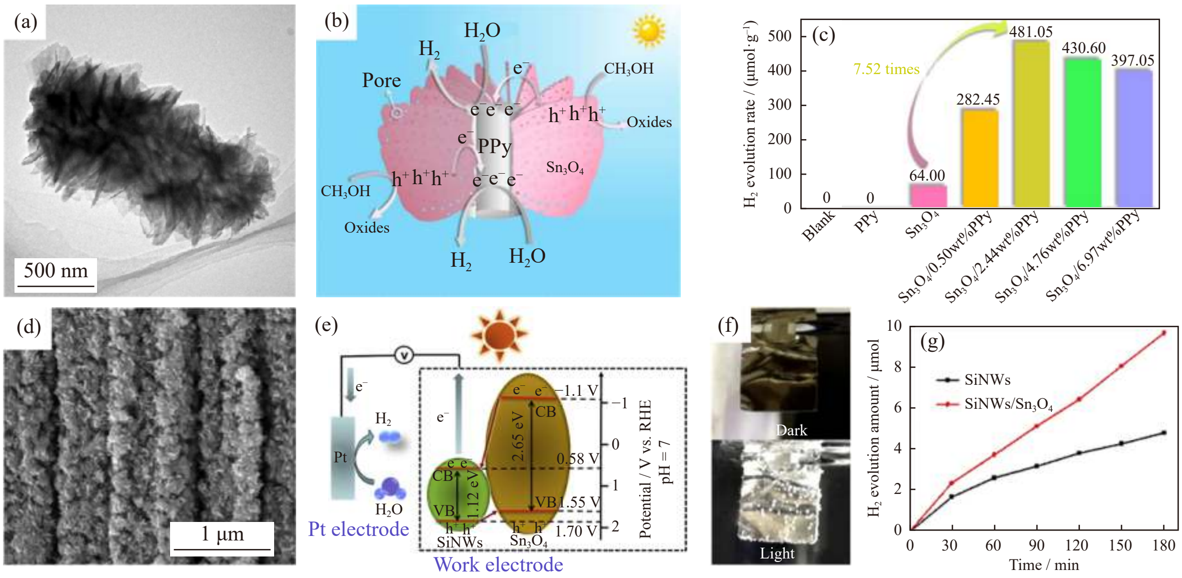

Fig. 5. (a) TEM image of Sn_3O_4/PPy heterostructure; (b) schematic of the plausible mechanism for the hydrogen photoevolution reaction catalyzed by Sn_3O_4/PPy heterostructure; (c) H_2 photoevolution of Sn_3O_4/PPy heterostructures. Reprinted from *Appl. Catal. B Environ.*, 279, L.Q. Yang, M.F. Lv, Y. Song, *et al.*, Porous Sn_3O_4 nanosheets on PPy hollow rod with photo-induced electrons oriented migration for enhanced visible-light hydrogen production, 119341, Copyright 2020, with permission from Elsevier; (d) SEM image of Sn_3O_4/Si heterostructure; (e) schematic of electron transfer in the Sn_3O_4/Si heterostructure; (f) photographs of H_2 generation on the Pt counter electrode: off-light and on-light conditions; (g) photoelectrocatalytic (PEC) H_2 generation of Sn_3O_4/Si heterostructure. Reprinted from *Appl. Catal. B Environ.*, 256, L.Q. Yang, Y.C. Ji, Q. Li, *et al.*, Ultrafine Si nanowires/Sn_3O_4 nanosheets 3D hierarchical heterostructured array as a photoanode with high-efficient photoelectrocatalytic performance, 117798, Copyright 2019, with permission from Elsevier.

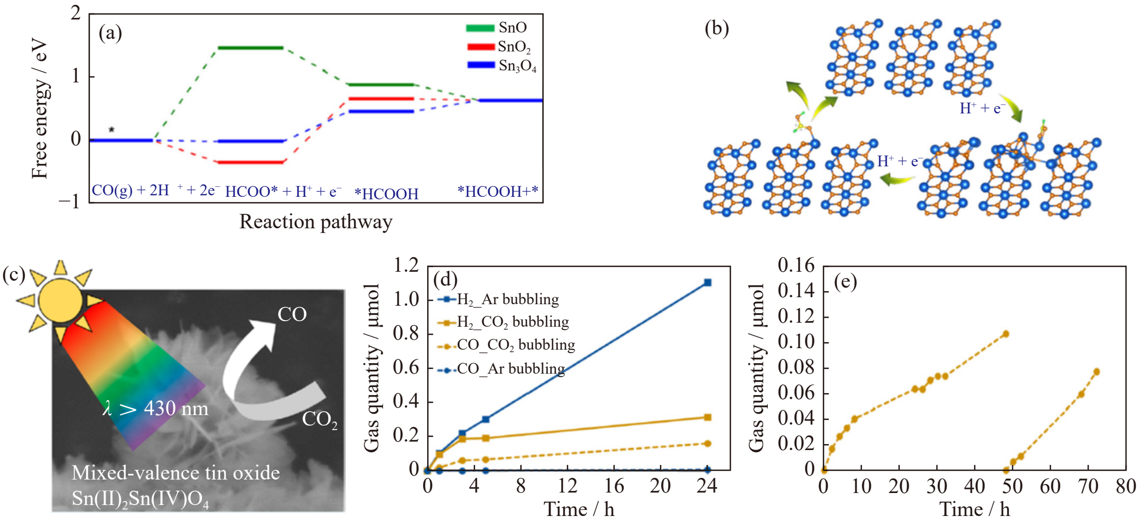

Fig. 6. (a) Free energy diagram of the CO_2 reduction reaction pathway to HCOOH on SnO, SnO_2, and Sn_3O_4; (b) schematic of the CO_2 reduction reaction process on Sn_3O_4. Color code: orange for oxygen, yellow for carbon, blue for tin, and green for hydrogen. Faraday efficiency of the target product (for interpretation of the references to color in the figure, the reader is referred to the web version of this article). Reprinted from *Appl. Catal. B Environ.*, 277, Z. Chen, M.R. Gao, N.Q. Duan,, *et al.*, Tuning adsorption strength of CO_2 and its intermediates on tin oxide-based electrocatalyst for efficient CO_2 reduction towards carbonaceous products, 119252, Copyright 2020, with permission from Elsevier; (c) schematic of photocatalytic reduction of CO_2 using Sn_3O_4; (d) photocatalytic CO_2 reduction properties under visible-light irradiation, with CO_2 (brown) and Ar (blue) bubbling; (e) CO evolution induced by Sn_3O_4 under visible-light irradiation during 72 h of irradiation. Reprinted with permission from Y.S. Liu, A. Yamaguchi, Y. Yang, *et al.*, *ACS Appl. Energy Mater.*, 4, 13415 [66]. Copyright 2021 American Chemical Society.

warrants further exploration. These findings participate in the advancement of CO_2 reduction research and offer valuable insights into potential applications of Sn_3O_4 as an efficient electrocatalyst and photocatalyst for CO_2 conversion.

5.4. Antibacterial therapy

Bacterial infections pose an important global public health challenge, affecting millions of individuals annually. This problem is exacerbated by the emergence of multidrug-resistant “superbugs” due to antibiotic misuse, necessitating the development of novel reagents and approaches for the treatment of bacterial infections [67]. Antibacterial photocatalytic therapy (APCT) is a promising treatment modality for drug-resistant bacterial infections, leveraging advances in optical technology and the development of photocatalytic materials [68–70]. However, the efficacy of PDT in *in vivo* antibacterial treatment is often compromised by the limited tissue penetration depth of the light source and low-oxygen microenvironment at the infection site.

Wang *et al.* [71] successfully prepared porous Sn_3O_x nanosheets *in-situ* with surface amorphous oxygen-rich vacancies on Ni foam through a simple hydrothermal method. These nanosheets demonstrated an enhanced photoelectrochemical sterilization performance. The porous structure of Sn_3O_x enriched the O vacancies on its surface and extended the absorption spectrum from visible light to the near-infrared region. Moreover, the oxygen vacancies boosted the effective separation of electron–hole pairs. Notably, the sheet-like porous structure increased the surface active sites and the contact area between the bacteria and the electrode. As a result, the ROS generated during the photoelectrochemical sterilization process can directly act on the bacterial surface. Remarkably, drug-resistant bacteria in water were completely eliminated within 30 min, achieving 100% efficiency (Fig. 7(a)–(b)).

Yang *et al.* [29] developed an innovative organic–inorganic hybrid Sn_3O_4/PDINH heterostructure for the photocatalytic generation of ROS to combat drug-resistant bacteria (Fig. 7(c)–(e)). The organic semiconductor PDINH was employed to self-assemble on the surface of Sn_3O_4 nanosheets via abundant hydrogen bonding and π–π stacking interactions. This self-assembly created a unique “hook-loop” adhesive surface that interacted with functional groups on the bacterial surface, resulting in their firm adherence to the bacteria. This hybrid heterostructure also exhibited a remarkably enhanced photocatalytic activity. Moreover, it showed an extended absorption spectrum up to 720 nm in the near-infrared region and effectively reduced the rate of photogenerated charge carrier recombination, thereby generating a high amount of ROS. The hybrid nanostructure was applied as an antibacterial coating on the skin surface for *in vivo* photocatalytic sterilization of a mouse model with *S. aureus*-infected skin wounds, and it considerably promoted the healing of infected skin wounds. This work presented a novel approach for the fabrication of full-spectrum organic–inorganic hybrid adhesive heterostructure photocatalysts with potential applications in wound infection treatment.

5.5. Solar cells

In the field of perovskite solar cells (PSCs), 2D mixed-valence tin oxide Sn_3O_4 has emerged as a promising electron transport layer (ETL) due to its low defect density and suitable band structure. Li *et al.* [72] reported the controllable synthesis of 2D van der Waals mixed-valence tin oxides

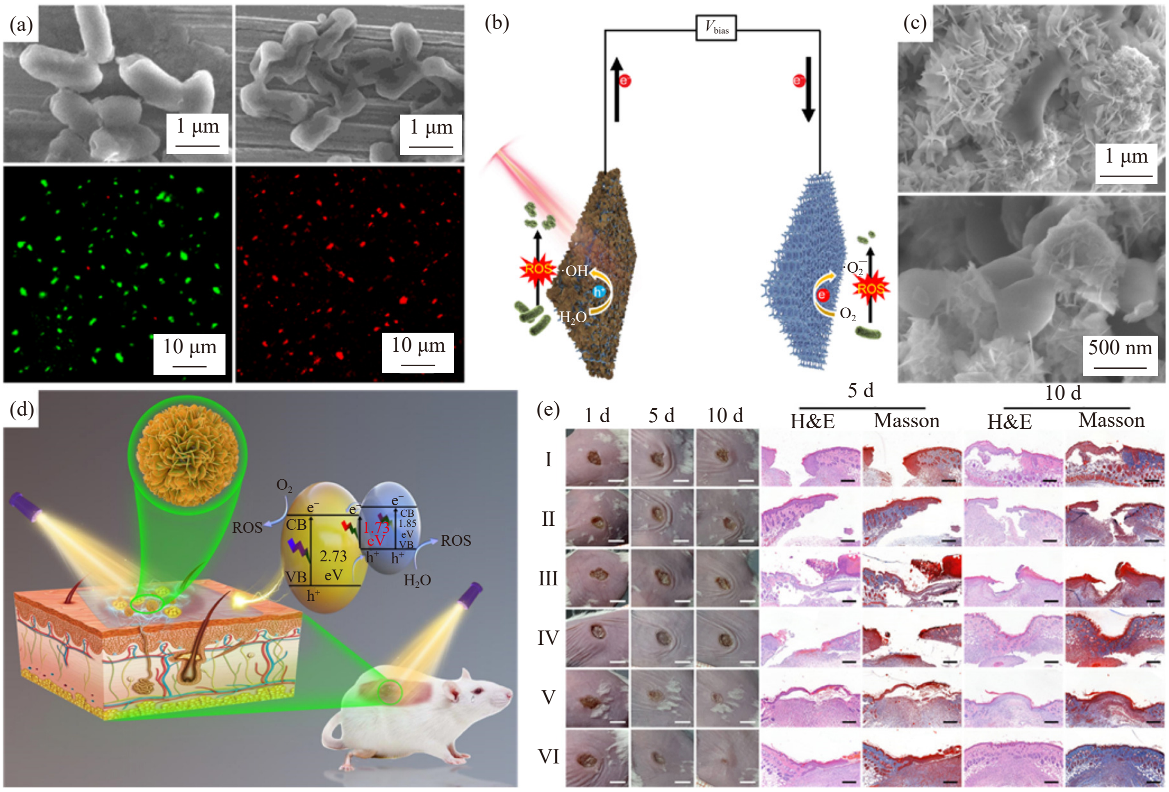

Fig. 7. (a) SEM images of Chl^r *E. coli* before and after PEC oxidation for 30 min and the corresponding fluorescence microscopic images; (b) schematic of Sn_3O_x/Ni foam photoanode. Reprinted by permission from Springer Nature: *Rare Met.*, Surface amorphization oxygen vacancy-rich porous Sn_3O_x nanosheets for boosted photoelectrocatalytic bacterial inactivation, L.W. Wang, L. Liu, Z. You, *et al.*, Copyright 2023; (c) SEM images of bacterial treatment with Sn_3O_4/PDINH heterostructure; (d) schematic of Sn_3O_4/PDINH APCT; (e) photographs of the infected wound treated on 1, 5, and 10 d and infected wound histologic analyses on days 5 and 10 at different treatments (I: phosphate-buffered saline (control), II: only light, III: Sn_3O_4/PDINH, IV: Sn_3O_4+light, V: PDINH+light, VI: Sn_3O_4/PDINH+light). The scale bar is 0.5 cm in the photographs and 400 μm in the histologic picture, respectively. R.Q. Yang, G.X. Song, L.W. Wang, *Small*, 17, e2102744 (2021) [29]. Copyright Wiley-VCH Verlag GmbH & Co. KGaA. Reproduced with permission.

(Sn_2O_3 and Sn_3O_4) and their application as electron transport materials in planar PSCs. The sizes of the synthesized Sn_2O_3 and Sn_3O_4 nanoparticles, which can be stably dispersed in water as colloids for several months, ranged from 5 to 20 nm (Fig. 8(a)–(b)). In addition, Sn_2O_3 and Sn_3O_4 demonstrated typical n-type semiconductor band structures, low trap densities, and appropriate energy level alignment with halide perovskites (Fig. 8(c)). According to experimental results, the steady-state power conversion efficiencies (PCEs) of Sn_2O_3-based and Sn_3O_4-based planar PSCs reached 22.36% and 21.83%, respectively (Fig. 8(d)).

Furthermore, the n-doping of Sn_3O_4 mixed-valence tin oxide through YCl_3 doping was explored to enhance its potential as an ETL in PSCs [73]. For Y doping levels below 10mol% (Y-to-Sn mol ratio), both products appeared as yellow colloids with good dispersibility in water (Fig. 8(e)). The Y-Sn_3O_4, with an optimal doping level of 5mol%, exhibited an elliptical shape with a length of approximately 20 nm and a thickness of approximately 5 nm (Fig. 8(f)). The doping level played a crucial role in the performance of Sn_3O_4 as excessive YCl_3 doping resulted in phase segregation along with the formation of SnO. However, at the 5mol% Y doping level, the electronic properties of Sn_3O_4 can be successfully optimized by increasing the electron density and conductivity and shifting the Fermi level upward (Fig. 8(g)). The optimized electronic performance, achieved through enhanced electron extraction and transport capabilities, and optimized energy level alignment in Sn_3O_4 considerably improved its potential as an ETL in PSCs. Consequently, the PSCs attained a PCE of 23.05% (Fig. 8(h)). These findings further highlight the application prospects of mixed-valence tin oxides in highly efficient PSCs.

5.6. Sensors

Considerable attention has been paid to photodetectors based on particularly self-powered photodetectors that eliminate the need for external power sources such as batteries. These self-powered devices show remarkable potential for high-sensitivity and high-speed applications. However, the fabrication of visible-light photodetectors remains a challenging task. Wang *et al.* [74] introduced a novel photovoltaic chemical platform based on Sn_3O_4, where Sn_3O_4 served as the active material for visible-light detection. A hydrothermal method was used to *in-situ* modify Sn_3O_4 nanosheets on the carbon fiber paper (CFP), and a molecularly imprinted polymer (MIP) layer with a specific selectivity for 2,4-dichlorophenoxyacetic acid (2,4-D) was synthesized on Sn_3O_4/CFP through the electropolymerization reaction of

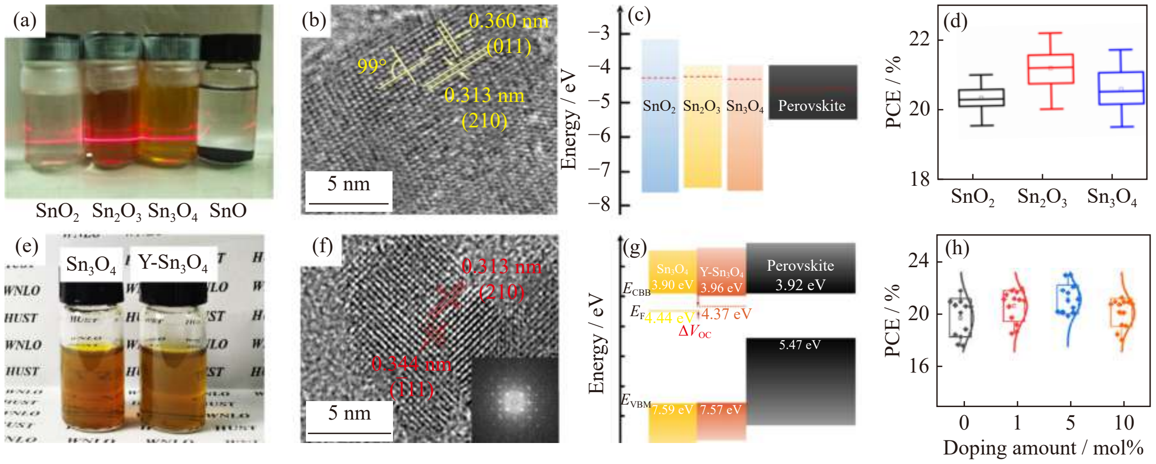

Fig. 8. (a) Photographs of SnO_2, Sn_2O_3, Sn_3O_4 dispersions, and SnO precipitation in water; (b) HRTEM image of Sn_3O_4 for phase identification; (c) band alignments with halide perovskites; (d) box plot of efficiency distribution values of PSCs based on SnO_2, Sn_2O_3, and Sn_3O_4 ETLs. Error bars represent the standard deviation. Reprinted with permission from S. Li, F. Qin, Q. Peng, *et al.*, *Nano Lett.*, 20, 8178 [72]. Copyright 2020 American Chemical Society; (e) photograph of Sn_3O_4 and Y-Sn_3O_4 dispersions in water; (f) HRTEM image and crystal labeling of Y-Sn_3O_4. The inset image shows the fast Fourier transform result; (g) band alignment of Sn_3O_4 and Y-Sn_3O_4 with perovskite; (h) efficiency distribution of devices corresponding to various Y-doping concentrations [73].

pyrrole in the presence of 2,4-D. 2,4-D was selected for the analysis due to its classification as a "potentially carcinogenic compound" for humans. The label-free photodetector leverages the structural advantages of Sn_3O_4/CFP and the selectivity of MIP and demonstrates a linear range of 5.0×10^{-11} to 1.0×10^{-7} mol·L^{-1} for 2,4-D and an exceptionally low detection limit of 1.08×10^{-11} mol·L^{-1}. This photovoltaic chemical platform exhibited outstanding stability, repeatability, ease of preparation, low cost, and an impressively low detection limit. In addition, the photovoltaic chemical sensor was integrated onto surfaces of various nonplanar shapes and sizes, given the flexibility and bendability of CFP, thereby expanding the application range of this material in sensor construction.

Xu *et al.* [75] used an improved hydrothermal method to synthesize vertically aligned Sn_3O_4 nanosheets on CFP and exploited them as self-powered photovoltaic chemical batteries for visible-light detection. The Sn_3O_4 nanosheets grew perpendicularly on the CFP and formed a dense and uniform distribution on its surface. The intersecting nanosheets created numerous mesopores measuring hundreds of nanometers (Fig. 9(a)). The enhanced photoresponse was attributed to the synergistic effect between the vertically grown Sn_3O_4 nanosheets and the CFP substrate. The vertically aligned nanosheets provided efficient active sites by exposing more catalytic sites to the electrolyte. Furthermore, the layered structure of Sn_3O_4 with mesopores enhanced light absorption as the incident light was scattered between the nanosheets

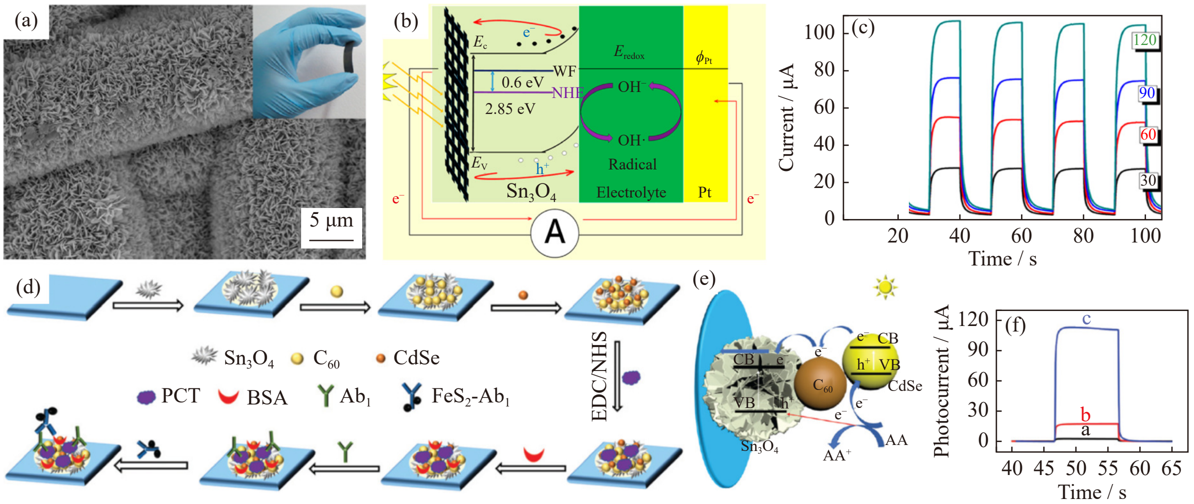

Fig. 9. (a) SEM image of hierarchical Sn_3O_4/carbon fiber heterostructure; (b) bandgap and V_O positions for Sn_3O_4; (c) photocurrent response under on/off cycling for 20 s at 0 V vs. Ag/AgCl for incident intensities equal to 30, 60, 90, and 120 mW·cm^{-2}. Reprinted with permission from W.W. Xia, H.Y. Qian, X.H. Zeng, J. Dong, J. Wang, and Q. Xu, *J. Phys. Chem. C*, 121, 19036 [75]. Copyright 2017 American Chemical Society; (d) construction process of the PEC sensor for procalcitonin (PCT) detection; (e) feasible mechanism of electron transfer of the PEC assay; (f) photocurrent of different electrodes. Republished with permission of Royal Society of Chemistry, from Antigen down format photoelectrochemical analysis supported by fullerene functionalized Sn_3O_4, R. Xu, Y. Du, D.Q. Leng, *et al.*, 56, 2020; permission conveyed through Copyright Clearance Center.

and captured by the mesopores. Light reflection was reduced in addition to enhanced light absorption. The CFP substrate contributed to the large surface area and facilitated charge and mass transfer (Fig. 9(b)).

The performance of the self-powered photovoltaic chemical batteries was evaluated using continuous visible-light pulses with varying intensities in alternating on/off cycles at specific time intervals. The photocurrent remained high after multiple on/off irradiation switching cycles. Moreover, the photocurrent increased with the increase in incident intensity (Fig. 9(c)). Compared with other self-powered devices that require binders, the in situ grown Sn_3O_4 electrodes on the CFP eliminated the need for binders, resulting in improved flexibility and performance, long-term stability, and easy recovery. Given its simplicity, cost-effectiveness, and environmentally friendly nature, this self-powered detector is highly promising for various applications in visible-light devices.

Wei *et al*. [76] proposed a novel competitive photovoltaic chemical sensor based on an Ag-down configuration (Fig. 9(d)). In this setup, a photosensitive material was immobilized on the electrode using a standard Ag method. Subsequently, specific immune reactions were induced for the comodification of the first antibody (Ab1) and the target Agon the electrode. Finally, the second antibody (Ab2) labeled with a suitable marker was immobilized. Fig. 9(e) depicts the possible mechanism of this configuration. The Sn_3O_4 material exhibited high photosensitivity, effectively absorbing visible light and displaying a satisfactory photoelectrochemical response. However, its relatively wide bandgap limited its potential for PEC analysis. To overcome this limitation, the researchers introduced C_{60}, a carbon nanostructure material known for its excellent photocatalytic performance. With its unique delocalized conjugated structure, C_{60} acted as an excellent electron acceptor, which enhanced charge separation and reduced the charge recombination of Sn_3O_4. As a result, the photocatalytic activity was improved. In addition, CdSe, an easily functionalized photosensitizer, was utilized to connect biomolecules. The cosensitization of C_{60} and CdSe enhanced the PEC response by more than five-fold compared with the pure material in the presence of ascorbic acid (Fig. 9(f)). This sensor demonstrated excellent sensitivity and stability, providing a powerful platform not only for the sensitive detection of PCT but also for the potential monitoring of other proteins.

6. Conclusions and future perspectives

Sn_3O_4 possesses thermodynamic stability and a bandgap within the visible light spectrum and shows promise as a visible-light-driven photocatalyst. This compound exhibits favorable properties, including suitable band edge positioning, low resistance, abundance, nontoxicity, and excellent photochemical stability in acidic and alkaline environments. Nonetheless, the low charge separation efficiency of pure Sn_3O_4 restricts its photocatalytic performance. This article presented a comprehensive overview of the latest advancements in the enhanced photocatalytic activity of Sn_3O_4. Various strategies, such as morphology control, ion doping, and heterostructure construction, have been employed for the design and fabrication of Sn_3O_4-based nanocomposites. The photocatalytic performances of these materials were thoroughly investigated, which led to their utilization in diverse applications, such as photocatalytic degradation, photocatalytic H_2 production, photocatalytic CO_2 reduction, photocatalytic disinfection, photovoltaics, and other related areas. Table 1 summarizes the latest functions and advantages of Sn_3O_4-based materials. The potential and research significance of Sn_3O_4-based photocatalytic materials extend to various fields. However, some issues remain to be addressed.

First, researchers have achieved considerable progress in

Table 1. Latest functions and advantages of Sn_3O_4-based materials

Materials	Application	Performance	Advantages	Ref.
Sn_3O_4/Sn	Degradation of pollutants	Rh b degradation	Oxygen vacancies; metal−semiconductor heterostructure; lower cytotoxicity	[53]
Sn_3O_4/Ni	Degradation of pollutants	PAM degradation	Metal−semiconductor heterostructure; photoelectrocatalysis	[59]
Sn_3O_4/TiO_2	Degradation of pollutants H_2 generation	MO degradation Water splitting	Semiconductor−semiconductor heterostructure; Janus heterostructure;	[33]
Ni-Sn_3O_4	H_2 generation	Water splitting	Enhanced crystallinity	[47]
Sn_3O_4/rGO	H_2 generation	Water splitting	Planar heterostructure; more catalytic active sites	[30]
Sn_3O_4/GQDs	H_2 generation	Water splitting	Mott−Schottky plots; GQDs as a photosensitizer	[56]
Sn_3O_4 nanoflowers	Reduction of CO_2	Reduction of CO_2 to CO	No cocatalysts	[66]
Sn_3O_4/PDINH	Antibacterial therapy	Inactivation of bacteria (*E. coli* and *S. aureus*)	Inorganic–organic heterostructure; capture bacteria	[29]
Sn_3O_x/Ni	Antibacterial activity	Inactivation of bacteria (*E. coli* and *S. aureus*)	Oxygen vacancies; photoelectrocatalysis	[71]
Y-Sn_3O_4	Solar cells	ETL for PSCs	High electron density; enhanced electron extraction capability	[73]
Sn_3O_4/CPF	Sensors	Visible-light detector	Large surface areas; good conductive channel for electron transport	[75]

the development of diverse and scalable approaches for the synthesis of Sn_3O_4 catalysts. However, the reproducible large-scale synthesis of Sn_3O_4 with precisely controlled morphology and composition remains a huge challenge. Further investigations must be conducted on the catalytically active surfaces of tin(IV) oxide and the crucial factors influencing its controllable synthesis. Under environmentally friendly conditions, the use of cost-effective and ecofriendly synthetic methods remains necessary.

Second, although the photocatalytic process involving Sn_3O_4 appears conceptually straightforward, its practical implementation is intricate and incompletely understood. Theoretical studies and *in-situ* surface chemistry research must be performed to gain insights into the intricate reactions of Sn_3O_4 and pave the way for the refinement and optimization of future catalyst designs.

Third, despite the immense potential of photocatalytic technology, the photovoltaic conversion efficiency of most Sn_3O_4-based semiconductor photocatalysts remains relatively low and thus must be improved. The modification of mixed-valence Sn_3O_4 presents a viable route to further enhance its photocatalytic performance. The use of advanced characterization techniques and computational studies is required for a comprehensive understanding of this aspect.

Last, compared with the studies on other materials, the research on Sn_3O_4 is relatively nascent, and its functionalities, effects, and applications require further exploration and advancements. Notably, properties resembling those of noble metals, surface plasmon resonance effects, influence of carriers, and organic reactions exhibit remarkable potential and merit extensive investigation. When harnessed effectively, these characteristics will play a pivotal role in photocatalytic applications.

Acknowledgements

The work was supported by the National Natural Science Foundation of China (No. 52272212), the Natural Science Foundation of Shandong Province (Nos. ZR2022JQ20 and ZR2023MB126), the Taishan Scholar Project of Shandong Province (No. tsqn202211168), the Key Laboratory of Optic-electric Sensing and Analytical Chemistry for Life Science, MOE (No. M2022-7), and the STIEI scientific research funding project (No. GCC2023036).

Conflict of Interest

The authors declare no competing financial interest.

References

[1] X. Yu, X. Jin, X.Y. Chen, *et al.*, A microorganism bred $TiO_2/Au/TiO_2$ heterostructure for whispering gallery mode resonance assisted plasmonic photocatalysis, *ACS Nano*, 14(2020), No. 10, p. 13876.

[2] Y.J. Fu, K.J. Zhang, Y. Zhang, Y.Q. Cong, and Q. Wang, Fabrication of visible-light-active MR/NH_2–MIL–125(Ti) homojunction with boosted photocatalytic performance, *Chem. Eng. J.*, 412(2021), art. No. 128722.

[3] Y.J. Fu, M. Tan, Z.L. Guo, *et al.*, Fabrication of wide-spectra-responsive NA/NH_2–MIL–125(Ti) with boosted activity for Cr(VI) reduction and antibacterial effects, *Chem. Eng. J.*, 452(2023), art. No. 139417.

[4] Q. Yang, M.L. Luo, K.W. Liu, H.M. Cao, and H.J. Yan, Covalent organic frameworks for photocatalytic applications, *Appl. Catal. B*, 276(2020), art. No. 119174.

[5] A. Mohammad, M.E. Khan, M.H. Cho, and T. Yoon, Adsorption promoted visible-light-induced photocatalytic degradation of antibiotic tetracycline by tin oxide/cerium oxide nanocomposite, *Appl. Surf. Sci.*, 565(2021), art. No. 150337.

[6] M. Honarmand, M. Golmohammadi, and A. Naeimi, Biosynthesis of tin oxide (SnO_2) nanoparticles using jujube fruit for photocatalytic degradation of organic dyes, *Adv. Powder Technol.*, 30(2019), No. 8, p. 1551.

[7] I. Fatimah, D. Rubiyanto, I. Sahroni, R.S. Putra, R. Nurillahi, and J. Nugraha, Physicochemical characteristics and photocatalytic performance of Tin oxide/montmorillonite nanocomposites at various Sn/montmorillonite molar to mass ratios, *Appl. Clay Sci.*, 193(2020), art. No. 105671.

[8] K. Balakrishnan, V. Veerapandy, H. Fjellvåg, and P. Vajeeston, First-principles exploration into the physical and chemical properties of certain newly identified SnO_2 polymorphs, *ACS Omega*, 7(2022), No. 12, p. 10382.

[9] Y.Q. Hu, J. Hwang, Y. Lee, *et al.*, First principles calculations of intrinsic mobilities in tin-based oxide semiconductors SnO, SnO_2, and Ta_2SnO_6, *J. Appl. Phys.*, 126(2019), No. 18, art. No. 185701.

[10] C. Wang, J.C. Zhao, X.M. Wang, *et al.*, Preparation, characterization and photocatalytic activity of nano-sized ZnO/SnO_2 coupled photocatalysts, *Appl. Catal. B*, 39(2002), No. 3, p. 269.

[11] T. Lu, Y.P. Zhang, H.B. Li, L.K. Pan, Y.L. Li, and Z. Sun, Electrochemical behaviors of graphene–ZnO and graphene–SnO_2 composite films for supercapacitors, *Electrochim. Acta*, 55(2010), No. 13, p. 4170.

[12] A. Seko, A. Togo, F. Oba, and I. Tanaka, Structure and stability of a homologous series of tin oxides, *Phys. Rev. Lett.*, 100(2008), No. 4, art. No. 045702.

[13] S. Das and V. Jayaraman, SnO_2: A comprehensive review on structures and gas sensors, *Prog. Mater. Sci.*, 66(2014), p. 112.

[14] C.Y. Sun, J.K. Yang, M. Xu, *et al.*, Recent intensification strategies of SnO_2-based photocatalysts: A review, *Chem. Eng. J.*, 427(2022), art. No. 131564.

[15] M.H. Chen, Z.C. Huang, G.T. Wu, G.M. Zhu, J.K. You, and Z.G. Lin, Synthesis and characterization of SnO–carbon nanotube composite as anode material for lithium-ion batteries, *Mater. Res. Bull.*, 38(2003), No. 5, p. 831.

[16] Y. Ogo, H. Hiramatsu, K. Nomura, *et al.*, P-channel thin-film transistor using p-type oxide semiconductor, SnO, *Appl. Phys. Lett.*, 93(2008), No. 3, art. No. 032113.

[17] R.Q. Yang, X. Yu, and H. Liu, Scientific study of photocatalytic material based on Sn_3O_4, *Chem. J. Chin. Univ.*, 42(2021), No. 5, p. 1340.

[18] L.P. Zhu, H. Lu, D. Hao, *et al.*, Three-dimensional lupinus-like TiO_2 nanorod@Sn_3O_4 nanosheet hierarchical heterostructured arrays as photoanode for enhanced photoelectrochemical performance, *ACS Appl. Mater. Interfaces*, 9(2017), No. 44, p. 38537.

[19] Q. Bai, J.C. Zhang, Y.X. Yu, *et al.*, Piezoelectric activatable nanozyme-based skin patch for rapid wound disinfection, *ACS Appl. Mater. Interfaces*, 14(2022), No. 23, p. 26455.

[20] Z.R. Dai, J.J. Lian, Y.S. Sun, *et al.*, Fabrication of g-C_3N_4/Sn_3O_4/Ni electrode for highly efficient photoelectrocatalytic reduction of U(VI), *Chem. Eng. J.*, 433(2022), art. No. 133766.

[21] T. Tanabe, K. Nakamori, T. Tanikawa, Y. Matsubara, and F. Matsumoto, Ultrathin nanosheet Sn_3O_4 for highly effective hydrogen evolution under visible light, *J. Photochem. Photobiol. A*, 420(2021), art. No. 113486.

[22] H. Song, S.Y. Son, S.K. Kim, and G.Y. Jung, A facile synthesis of hierarchical Sn_3O_4 nanostructures in an acidic aqueous solution and their strong visible-light-driven photocatalytic activity, *Nano Res.*, 8(2015), No. 11, p. 3553.

[23] J.J. Wang, N. Umezawa, and H. Hosono, Mixed valence tin oxides as novel van der Waals materials: Theoretical predictions and potential applications, *Adv. Energy Mater.*, 6(2016), No. 1, art. No. 1501190.

[24] M. Manikandan, T. Tanabe, P. Li, *et al.*, Photocatalytic water splitting under visible light by mixed-valence Sn_3O_4, *ACS Appl. Mater. Interfaces*, 6(2014), No. 6, p. 3790.

[25] Y.S. Liu, A. Yamaguchi, Y. Yang, *et al.*, Synthesis and characterization of the orthorhombic Sn_3O_4 polymorph, *Angew. Chem. Int. Ed*, 62(2023), No. 17, art. No. e202300640.

[26] C. Jose Damaschio, O.M. Berengue, D.G. Stroppa, *et al.*, Sn_3O_4 single crystal nanobelts grown by carbothermal reduction process, *J. Cryst. Growth*, 312(2010), No. 20, p. 2881.

[27] L.N. Zhang, X.Y. Liu, X. Zhang, *et al.*, Sulfur-doped Sn_3O_4 nanosheets for improved photocatalytic performance, *J. Alloys Compd.*, 961(2023), art. No. 170904.

[28] N. Yuan, X.L. Zhang, B.W. Li, T.X. Chen, and X. Yang, Energy-efficient MIL–53(Fe)/Sn_3O_4 nanosheet photocatalysts for visible-light degradation of toxic organics in wastewater, *ACS Appl. Nano Mater.*, 6(2023), No. 11, p. 9159.

[29] R.Q. Yang, G.X. Song, L.W. Wang, *et al.*, Full solar-spectrum-driven antibacterial therapy over hierarchical Sn_3O_4/PDINH with enhanced photocatalytic activity, *Small*, 17(2021), No. 39, art. No. e2102744.

[30] X. Yu, Z.H. Zhao, D.H. Sun, *et al.*, Microwave-assisted hydrothermal synthesis of Sn_3O_4 nanosheet/rGO planar heterostructure for efficient photocatalytic hydrogen generation, *Appl. Catal. B*, 227(2018), p. 470.

[31] X. Yu, J. Zhang, Z.H. Zhao, *et al.*, NiO–TiO_2 p–n heterostructured nanocables bridged by zero-bandgap rGO for highly efficient photocatalytic water splitting, *Nano Energy*, 16(2015), p. 207.

[32] X. Yu, X. Han, Z.H. Zhao, *et al.*, Hierarchical TiO_2 nanowire/graphite fiber photoelectrocatalysis setup powered by a wind-driven nanogenerator: A highly efficient photoelectrocatalytic device entirely based on renewable energy, *Nano Energy*, 11(2015), p. 19.

[33] X. Yu, L.F. Wang, J. Zhang, *et al.*, Hierarchical hybrid nanostructures of Sn_3O_4 on N doped TiO_2 nanotubes with enhanced photocatalytic performance, *J. Mater. Chem. A*, 3(2015), No. 37, p. 19129.

[34] X. Yu, N. Ren, J.C. Qiu, D.H. Sun, L.L. Li, and H. Liu, Killing two birds with one stone: To eliminate the toxicity and enhance the photocatalytic property of CdS nanobelts by assembling ultrafine TiO_2 nanowires on them, *Sol. Energy Mater. Sol. Cells*, 183(2018), p. 41.

[35] X. Yu, Z.H. Zhao, D.H. Sun, *et al.*, TiO_2/TiN core/shell nanobelts for efficient solar hydrogen generation, *Chem. Commun.*, 54(2018), No. 47, p. 6056.

[36] Y.C. Ji, R.Q. Yang, L.W. Wang, *et al.*, Visible light active and noble metal free Nb_4N_5/TiO_2 nanobelt surface heterostructure for plasmonic enhanced solar water splitting, *Chem. Eng. J.*, 402(2020), art. No. 126226.

[37] H.X. Liu, M.Y. Teng, X.G. Wei, *et al.*, Mosaic structure ZnO formed by secondary crystallization with enhanced photocatalytic performance, *Int. J. Miner. Metall. Mater.*, 28(2021), No. 3, p. 495.

[38] .M. Berengue, R.A. Simon, A.J. Chiquito, *et al.*, Semiconducting Sn_3O_4 nanobelts: Growth and electronic structure, *J. Appl. Phys.*, 107(2010), No. 3, art. No. 033717.

[39] P. Mone, S. Mardikar, and S. Balgude, Morphology-controlled synthesis of Sn_3O_4 nanowires for enhanced solar-light driven photocatalytic H_2 production, *Nano Struct. Nano Objects*, 24(2020), art. No. 100615.

[40] Y.H. He, D.Z. Li, J. Chen, *et al.*, Sn_3O_4: A novel heterovalent-tin photocatalyst with hierarchical 3D nanostructures under visible light, *RSC Adv.*, 4(2014), No. 3, p. 1266.

[41] S. Balgude, Y. Sethi, B. Kale, D. Amalnerkar, and P. Adhyapak, Sn_3O_4 microballs as highly efficient photocatalyst for hydrogen generation and degradation of phenol under solar light irradiation, *Mater. Chem. Phys.*, 221(2019), p. 493.

[42] X.H. Ma, J.L. Shen, D.X. Hu, *et al.*, Preparation of three-dimensional Ce-doped Sn_3O_4 hierarchical microsphere and its application on formaldehyde gas sensor, *J. Alloys Compd.*, 726(2017), p. 1092.

[43] S. Balgude, Y. Sethi, A. Gaikwad, B. Kale, D. Amalnerkar, and P. Adhyapak, Unique N doped Sn_3O_4 nanosheets as an efficient and stable photocatalyst for hydrogen generation under sunlight, *Nanoscale*, 12(2020), No. 15, p. 8502.

[44] D.B. Zeng, C.L. Yu, Q.Z. Fan, *et al.*, Theoretical and experimental research of novel fluorine doped hierarchical Sn_3O_4 microspheres with excellent photocatalytic performance for removal of Cr(VI) and organic pollutants, *Chem. Eng. J.*, 391(2020), art. No. 123607.

[45] C.L. Yu, D.B. Zeng, Q.Z. Fan, *et al.*, The distinct role of boron doping in Sn_3O_4 microspheres for synergistic removal of phenols and Cr(VI) in simulated wastewater, *Environ. Sci. Nano*, 7(2020), No. 1, p. 286.

[46] L. Wang, Y. Li, W.J. Yue, S. Gao, C.W. Zhang, and Z.X. Chen, High-performance formaldehyde gas sensor based on Cu-doped Sn_3O_4 hierarchical nanoflowers, *IEEE Sens. J.*, 20(2020), No. 13, p. 6945.

[47] R.Q. Yang, Y.C. Ji, L.W. Wang, *et al.*, Crystalline Ni-doped Sn_3O_4 nanosheets for photocatalytic H_2 production, *ACS Appl. Nano Mater.*, 3(2020), No. 9, p. 9268.

[48] Z.R. Liu, L.W. Wang, X. Yu, *et al.*, Piezoelectric-effect-enhanced full-spectrum photoelectrocatalysis in p–n heterojunction, *Adv. Funct. Mater.*, 29(2019), No. 41, art. No. 1807279.

[49] X. Yu, S. Wang, X.D. Zhang, *et al.*, Heterostructured nanorod array with piezophototronic and plasmonic effect for photodynamic bacteria killing and wound healing, *Nano Energy*, 46(2018), p. 29.

[50] J.S. Yuan, Y. Zhang, X.Y. Zhang, J.J. Zhang, and S.G. Zhang, N-doped graphene quantum dots-decorated N-TiO_2/P-doped porous hollow g-C_3N_4 nanotube composite photocatalysts for antibiotics photodegradation and H_2 production, *Int. J. Miner. Metall. Mater.*, 31(2024), No. 1, p. 165.

[51] Y. Wen, D.D. Wang, H.J. Li, *et al.*, Enhanced photocatalytic hydrogen evolution of 2D/2D N-Sn_3O_4/g-C_3N_4 S-scheme heterojunction under visible light irradiation, *Appl. Surf. Sci.*, 567(2021), art. No. 150903.

[52] X. Jiang, M.T. Wang, B.N. Luo, *et al.*, Magnetically recoverable flower-like Sn_3O_4/$SnFe_2O_4$ as a type-II heterojunction photocatalyst for efficient degradation of ciprofloxacin, *J. Alloys Compd.*, 926(2022), art. No. 166878.

[53] R.Q. Yang, N. Liang, X.Y. Chen, *et al.*, Sn/Sn_3O_{4-x} heterostructure rich in oxygen vacancies with enhanced visible light photocatalytic oxidation performance, *Int. J. Miner. Metall. Mater.*, 28(2021), No. 1, p. 150.

[54] H.H. Wang, W.X. Liu, J. Ma, *et al.*, Design of (GO/TiO_2)N one-dimensional photonic crystal photocatalysts with improved photocatalytic activity for tetracycline degradation, *Int. J. Miner. Metall. Mater.*, 27(2020), No. 6, p. 830.

[55] F.C. Wen, S.R.G.G. Li, Y. Chen, *et al.*, Corrugated rGO-supported Pd composite on carbon paper for efficient cathode of Mg–H_2O_2 semi-fuel cell, *Rare Met.*, 41(2022), No. 8, p. 2655.

[56] X. Yu, Z.H. Zhao, N. Ren, *et al.*, Top or bottom, assembling modules determine the photocatalytic property of the sheetlike nanostructured hybrid photocatalyst composed with Sn_3O_4 and rGO (GQD), *ACS Sustainable Chem. Eng.*, 6(2018), No. 9, p. 11775.

[57] X.F. Zeng, J.S. Wang, Y.N. Zhao, W.L. Zhang, and M.H. Wang, Construction of TiO_2-pillared multilayer graphene nanocomposites as efficient photocatalysts for ciprofloxacin degradation, *Int. J. Miner. Metall. Mater.*, 28(2021), No. 3, p. 503.

[58] H.M. Shao, X.Y. Shen, X.T. Li, *et al.*, Growth mechanism and photocatalytic evaluation of flower-like ZnO micro-structures prepared with SDBS assistance, *Int. J. Miner. Metall. Mater.*, 28(2021), No. 4, p. 729.

[59] R.Q. Yang, Y.C. Ji, J. Zhang, *et al.*, Efficiently degradation of polyacrylamide pollution using a full spectrum Sn_3O_4 nanosheet/Ni foam heterostructure photoelectrocatalyst, *Catal. Today*, 335(2019), p. 520.

[60] Y.Q. Han, M.M. Wei, S.Y Qu, *et al.*, Ag@AgCl quantum dots embedded on Sn_3O_4 nanosheets towards synergistic 3D flower-like heterostructured microspheres for efficient visible-lkght photocatalysis, *Ceram. Int.*, 46 (2020), No. 15, p. 24060.

[61] L. Chen, S. Yue, J. Wang, *et al.*, Overall water splitting on surface-polarized Sn_3O_4 through weakening the trap of Sn(II) to holes, *Appl. Catal. B*, 299(2021), art. No. 120689.

[62] L. Xu, W.Q. Chen, S.Q. Ke, *et al.*, Construction of heterojunction $Bi/Bi_5O_7I/Sn_3O_4$ for efficient noble-metal-free Z-scheme photocatalytic H_2 evolution, *Chem. Eng. J.*, 382(2020), art. No. 122810.

[63] L.Q. Yang, M.F. Lv, Y. Song, *et al.*, Porous Sn_3O_4 nanosheets on PPy hollow rod with photo-induced electrons oriented migration for enhanced visible-light hydrogen production, *Appl. Catal. B*, 279(2020), art. No. 119341.

[64] R.Q. Yang, Y.C. Ji, Q. Li, *et al.*, Ultrafine Si nanowires/Sn_3O_4 nanosheets 3D hierarchical heterostructured array as a photoanode with high-efficient photoelectrocatalytic performance, *Appl. Catal. B*, 256(2019), art. No. 117798.

[65] Z. Chen, M.R. Gao, N.Q. Duan, *et al.*, Tuning adsorption strength of CO_2 and its intermediates on tin oxide-based electrocatalyst for efficient CO_2 reduction towards carbonaceous products, *Appl. Catal. B*, 277(2020), art. No. 119252.

[66] Y.S. Liu, A. Yamaguchi, Y. Yang, *et al.*, Visible-light-induced CO_2 reduction by mixed-valence tin oxide, *ACS Appl. Energy Mater.*, 4(2021), No. 12, p. 13415.

[67] L.W. Wang, F.E. Gao, A.Z. Wang, *et al.*, Defect-rich adhesive molybdenum disulfide/rGO vertical heterostructures with enhanced nanozyme activity for smart bacterial killing application, *Adv. Mater.*, 32(2020), No. 48, art. No. e2005423.

[68] L.W. Wang, X.W. Tang, Z.W. Yang, *et al.*, Regulation of functional groups enable the metal-free PDINH/GO advisable antibacterial photocatalytic therapy, *Chem. Eng. J.*, 451(2023), art. No. 139007.

[69] L.W. Wang, Z.W. Yang, G.X. Song, *et al.*, Construction of S–N–C bond for boosting bacteria-killing by synergistic effect of photocatalysis and nanozyme, *Appl. Catal. B*, 325(2023), art. No. 122345.

[70] L.W. Wang, X. Zhang, X. Yu, *et al.*, An all-organic semiconductor C_3N_4/PDINH heterostructure with advanced antibacterial photocatalytic therapy activity, *Adv. Mater.*, 31(2019), No. 33, art. No. 1901965.

[71] L.W. Wang, L. Liu, Z. You, *et al.*, Surface amorphization oxygen vacancy-rich porous Sn_3O_x nanosheets for boosted photoelectrocatalytic bacterial inactivation, *Rare Met.*, 42(2023), No. 5, p. 1508.

[72] S. Li, F. Qin, Q. Peng, *et al.*, Van der waals mixed valence tin oxides for perovskite solar cells as UV-stable electron transport materials, *Nano Lett.*, 20(2020), No. 11, p. 8178.

[73] S. Li, J.L. Liu, S. Liu, *et al.*, Yttrium-doped Sn_3O_4 two-dimensional electron transport material for perovskite solar cells with efficiency over 23%, *EcoMat*, 4(2022), No. 4, art. No. e12202.

[74] J. Wang, Q. Xu, W.W. Xia, *et al.*, High sensitive visible light photoelectrochemical sensor based on *in situ* prepared flexible Sn_3O_4 nanosheets and molecularly imprinted polymers, *Sens. Actuators B*, 271(2018), p. 215.

[75] W.W. Xia, H.Y. Qian, X.H. Zeng, J. Dong, J. Wang, and Q. Xu, Visible-light self-powered photodetector and recoverable photocatalyst fabricated from vertically aligned Sn_3O_4 nanoflakes on carbon paper, *J. Phys. Chem. C*, 121(2017), No. 35, p. 19036.

[76] R. Xu, Y. Du, D.Q. Leng, *et al.*, Antigen down format photoelectrochemical analysis supported by fullerene functionalized Sn_3O_4, *Chem. Commun.*, 56(2020), No. 54, p. 7455.